Room-temperature continuous-wave vertical-cavity surface-emitting lasers based on 2D layered organic–inorganic hybrid perovskites

Zhang, Hongbo; Hu, Yuzhong; Wen, Wen; Du, Bowen; Wu, Lishu; Chen, Yu; Feng, Shun; Zou, Chenji; Shang, Jingzhi; Fan, Hong Jin; Yu, Ting

2021

Zhang, H., Hu, Y., Wen, W., Du, B., Wu, L., Chen, Y., Feng, S., Zou, C., Shang, J., Fan, H. J. & Yu, T. (2021). Room-temperature continuous-wave vertical-cavity surface-emitting lasers based on 2D layered organic–inorganic hybrid perovskites. APL Materials, 9(7), 071106-. https://dx.doi.org/10.1063/5.0052458

https://hdl.handle.net/10356/151912

https://doi.org/10.1063/5.0052458

APL Materials

Room-temperature continuous-wave vertical-cavity surface-emitting lasers based on 2D layered organic–inorganic hybrid perovskites

Cite as: APL Mater. 9, 071106 (2021); https://doi.org/10.1063/5.0052458
Submitted: 31 March 2021 . Accepted: 16 June 2021 . Published Online: 02 July 2021

Hongbo Zhang, Yuzhong Hu, Wen Wen, Bowen Du, Lishu Wu, Yu Chen, Shun Feng, Chenji Zou, Jingzhi Shang, Hong Jin Fan, and Ting Yu

AIP Publishing

Room-temperature continuous-wave vertical-cavity surface-emitting lasers based on 2D layered organic–inorganic hybrid perovskites

Cite as: APL Mater. 9, 071106 (2021); doi: 10.1063/5.0052458
Submitted: 31 March 2021 • Accepted: 16 June 2021 •
Published Online: 2 July 2021

Hongbo Zhang,[1] Yuzhong Hu,[1] Wen Wen,[1] Bowen Du,[1] Lishu Wu,[1] Yu Chen,[1,2] Shun Feng,[1,3] Chenji Zou,[1] Jingzhi Shang,[4,a)] Hong Jin Fan,[1,a)] and Ting Yu[1,a)]

AFFILIATIONS

[1] Division of Physics and Applied Physics, School of Physical and Mathematical Sciences, Nanyang Technological University, Singapore 637371, Singapore
[2] Commonwealth Scientific and Industrial Research Organisation (CSIRO) Manufacturing, Clayton, Victoria 3168, Australia
[3] Institute of Photonics and Quantum Sciences, SUPA, Heriot-Watt University, Edinburgh EH14 4AS, United Kingdom
[4] Shaanxi Institute of Flexible Electronics (SIFE), Northwestern Polytechnical University (NPU), Xi'an 710129, China

Note: This paper is part of the Special Topic on 2D Materials Chemistry.
[a)] **Authors to whom correspondence should be addressed:** iamjzshang@nwpu.edu.cn; fanhj@ntu.edu.sg; and yuting@ntu.edu.sg

ABSTRACT

Two-dimensional (2D) layered lead halide perovskites with large exciton binding energies, efficient radiative recombination, and outstanding environmental stability are regarded as supreme candidates for realizing highly compact and ultralow threshold lasers. However, continuous-wave (CW) pumped lasing of 2D lead halide perovskites, as the precondition for the electrically pumped lasing, is still challenging. Here, we tackled this challenge by demonstrating lasing emission in phenylethylammonium lead iodide [$(PEA)_2PbI_4$] embedded in a vertical microcavity under continuous pumping at room temperature. The millimeter-sized $(PEA)_2PbI_4$ single crystal was obtained from a two-step seed-growth method, showing high crystallization, excellent thermal stability, and outstanding optical properties. We used the exfoliated $(PEA)_2PbI_4$ thin flake as the gain medium to construct a vertical-cavity surface-emitting laser (VCSEL), showing robust single-mode CW lasing operation with an ultra-low threshold of 5.7 W cm^{-2} at room temperature, attributed to strong optical confinement in the high-Q cavity. Our findings provide a strategy to design and fabricate solution-based 2D perovskite VCSELs and mark a significant step toward the next-generation of coherent light sources.

Organic–inorganic metal halide perovskites have blossomed into a fantastic family of semiconducting materials on account of their extraordinary optoelectronic performances in photovoltaics,[1] photodetectors,[2,3] and light-emitting devices.[4] Recently, 2D layered organic–inorganic perovskites have aroused much attention owing to their outstanding environmental stability.[5] The general chemical formula for the 2D organic–inorganic perovskites is $R_2A_{n-1}Pb_nX_{3n+1}$, where R represents long organic chains, such as phenylethylammonium (PEA^+), 1-naphthylmethylamine (NMA^+), and *n*-butylammonium (BA^+); A means the organic/inorganic cation, such as methylammonium (MA^+), formamidinium (FA^+), and cesium (Cs^+); and X can be a halide anion, such as iodide (I^-), bromide (Br^-), or chloride (Cl^-).[6] For n > 1, multilayered small cations (A) form quasi-2D perovskites, and for n = 1, two long-chain layers and one inorganic $[PbX_6]^{4-}$ form a molecularly thin 2D structure.[7] The variations of n values affect the bandgaps and binding energies of the materials due to different quantum confinement effects of self-built multiple-quantum-well structures. In particular, the excitons in 2D organic–inorganic perovskites own a robust electrostatic Coulomb coupling and small Bohr radius, leading to their distinct optical properties, such as large exciton binding energy, effective quantum yield, and efficient radiative recombination.[5]

Thanks to these brilliant properties, 2D layer organic–inorganic perovskites are superior candidates for the gain medium in practical lasing applications in the integrated optical circuit, quantum communication, and quantum computing.

Recently, the amplified spontaneous emission (ASE) and lasing emissions (LEs) of 2D organic–inorganic perovskites have been intensively studied.[8–11] For example, Li *et al.* have reported the tunable ASE in hybrid $(NMA)_2(FA)Pb_2Br_yI_{7-y}$ thin films.[12] Using NMA-based 2D perovskite films as gain media, Leyden *et al.* reported distributed feedback (DFB) lasers and LEDs at room temperature.[13] By fabricating micro-ring arrays based on the 2D $(BA)_2(MA)_{n-1}Pb_nBr_{3n+1}$ perovskite thin film, high Q-factor whispering gallery mode lasers have been realized.[14] However, the lasing was mainly observed from solution-processed thin films, consisting of a mixture of domains having components with different n values, which leads to different bandgaps, and the energy funneling from small n domains (high bandgaps) to large n domains (low bandgaps) contributes to the build-up of population inversion. The investigation of pure phase 2D organic–inorganic perovskites is necessary for further understanding of inherent lasing mechanisms. In addition, achieving continuous-wave (CW) pumped lasing from 2D perovskites is still challenging, which is regarded as a precondition toward the electrically pumped laser.[15] Nevertheless, only limited studies for pulse pumped lasing from single-crystalline 2D perovskites have been tried. Raghavan *et al.* reported that the random lasing from the millimeter-sized homologous $(BA)_2(MA)_{n-1}Pb_nI_{3n+1}$ (n = 1, 2, and 3) single crystals at room temperature attributes to the multiple scatterings from the resonant feedback formed by gain media.[16] Yin *et al.* demonstrated broadly tunable lasing from exfoliated single-crystalline BA-based 2D perovskite thin flakes at cryogenic temperature.[17] Due to the weak van der Waals interactions among the organic layers, the 2D perovskites are appropriately exfoliated and transferred to the substrates without requirement of the lattice matching, which is in favor of device fabrication. In sharp contrast to cavity-free perovskite lasers based on the 2D PEABr and NMABr perovskite thin-film spin-coated on distributed feedback gratings,[18] due to low defect densities of single-crystalline 2D perovskites and their self-built quantum well structures, 2D perovskite embedded microcavities with the matched resonance between the spontaneous emission and the cavity mode are the promising device architectures to achieve CW lasing with low threshold and high stability at room temperature.

In this work, we have realized CW lasing from a single-crystalline $(PEA)_2PbI_4$ flake embedded microcavity at room temperature. Owing to the high crystal quality of the $(PEA)_2PbI_4$ and ultrathin cavity, a single-mode lasing emission has been observed at an ultra-low threshold of 5.7 W cm^{-2}, which is generally lower than the lasing threshold values reported in existing 2D perovskite lasers.[18] The apparent features of spectral linewidth narrowing and nonlinear evolution of the emission intensity reveal the occurrence of lasing emission. Meanwhile, the fabricated $(PEA)_2PbI_4$ vertical-cavity surface-emitting laser (VCSEL) exhibits environmental and optical stability. Our results not only advance the development of 2D single-crystalline perovskite planar VCSELs but also shed light on the next-generation of on-chip integrated photonics.

The 2D layer $(PEA)_2PbI_4$ $[(C_6H_5C_2H_4NH_3)_2PbI_4]$ single crystal was fabricated in a modified seed-growth approach,[19] which includes two typical crystallization procedures of nucleation and growth. In particular, unlike the previous growth process using γ-butyrolactone (GBL) as the dissolving solvent, which usually requires a step of heating up to 110 °C,[20] the operation of the seed-growth approach is simpler and safer with a comparable gentle condition (90 °C). Structurally, the inorganic layer of $(PEA)_2PbI_4$ is formed by the arrangement of $[PbI_6]^{4-}$ octahedra, which share corners in their orthogonal directions. This inorganic lead-halide layer is separated from each other by two organic layers formed by long-chain PEA^+ cations, as shown in Fig. 1(a). The connection between the organic layer and the inorganic layer is attributed to the $H_N\cdots I$ hydrogen bond, while the interaction between two adjacent organic layers is owing to the weak van der Waals force.[21] Therefore, such a hybrid perovskite owns a two-dimensional layered structure, which allows us to mechanically exfoliate the bulk crystal to the thin flake.

The thermal stability of this crystal was studied by the thermogravimetric analysis (TGA) system. As shown in Fig. S2(a), this material gets no decomposition until ~190 °C, which means that the $(PEA)_2PbI_4$ single crystal has excellent stability at room temperature. X-ray diffraction (XRD) is a useful instrument to get vision into the crystal structure of crystalline materials. We performed the XRD examination of an as-prepared $(PEA)_2PbI_4$ single crystal with the (00n) crystal direction perpendicular to the measurement stage. As shown in Fig. 1(b), the observed positions of these fingerprinting peaks show the right consistency with the previous studies,[22] and the sharp shape of each peak indicates the good crystal quality of $(PEA)_2PbI_4$. The strongest peak located at $2\theta = 5.38°$ corresponds to the (002) plane, suggesting an interplanar distance of 1.65 nm. Thus, the thickness of a single layer $(PEA)_2PbI_4$ can be estimated.[23]

A representative optical image of exfoliated $(PEA)_2PbI_4$ flakes is presented in Fig. 1(d), with the relatively large size of several micrometers. In particular, the optical contrast of the $(PEA)_2PbI_4$ can reflect its thickness, which originates from the interference between the sample and the substrate.[24] The region in purple represents thinner samples, while the area in yellow represents a much thicker location (i.e., hundreds of nanometers). The AFM image and the corresponding height profile are shown in Figs. 1(e) and 1(f), respectively, where the thickness of the thin region is 175 nm. The optical image and AFM image of the thinner flake are shown in Fig. S3. The Raman spectrum excited by a 633 nm CW laser is shown in Fig. S2(b), where the dominant peak is located at 106 cm^{-1}. Coincident with the previous studies, this peak is ascribed to the π–π vibration of PEA rings.[25] The modes of in-plane Pb–I stretching, out-of-plane I–Pb–I rocking, and octahedral rotation, which were demonstrated locating at the frequency smaller than 60 cm^{-1},[26] were not recorded here due to the cutoff of Rayleigh scattering by our long-pass filter. In addition, under the excitation of a 488 nm CW laser at room temperature, the $(PEA)_2PbI_4$ flake exhibits the PL emission with a narrow linewidth of 13.5 nm at 527.1 nm [Fig. 1(c)], which is corresponding to an excitonic emission at 2.36 eV and indicates the high quality of the crystals.[2] The average PL lifetime for the $(PEA)_2PbI_4$ thin flake is 3.48 ns (Fig. S5), and the estimation of binding energy is 226 meV (Fig. S6). Due to such robust excitonic emission, the $(PEA)_2PbI_4$ flake can be unambiguously employed as an optical gain medium for further lasing investigation.

To realize efficient lasing emission, the most important consideration is sufficient optical gain and affordable losses of the cavity.

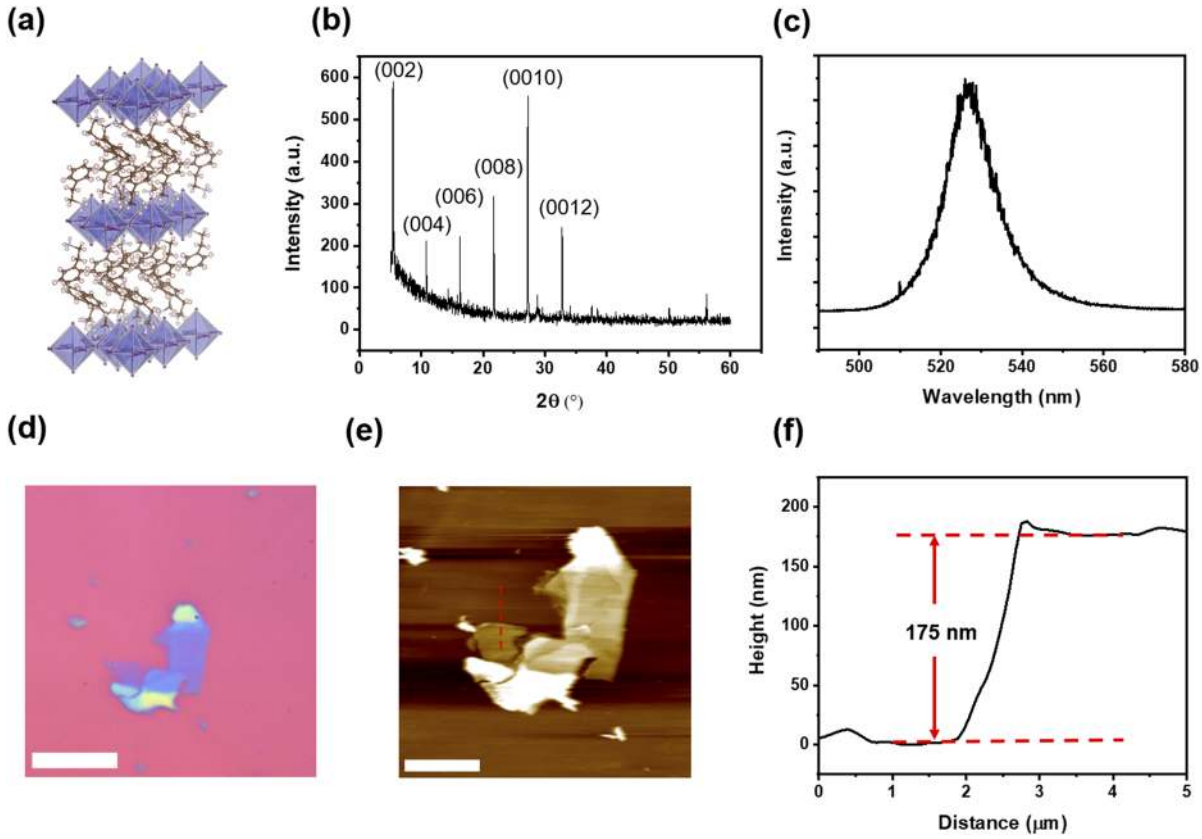

FIG. 1. Morphological and optical characterization of the prepared $(PEA)_2PbI_4$. (a) Schematic illustration of the optimized crystal structure of 2D layered $(PEA)_2PbI_4$ crystals along the C axis. (b) The XRD patterns of the $(PEA)_2PbI_4$ bulk crystal recorded from the (001) plane. (c) PL spectrum of the exfoliated $(PEA)_2PbI_4$ flake at room temperature. The emission peak is at 527.1 nm. (d) Optical image and (e) Atomic Force Microscope (AFM) image of the exfoliated $(PEA)_2PbI_4$ flake on the SiO_2 substrate. (f) The corresponding height profile of the selected zone in (e). Scale bar: 10 μm for (d) and 5 μm for (e).

In general, high reflectivity distributed Bragg reflectors (DBRs) are the prerequisite to realize in a vertical-cavity surface-emitting laser. As illustrated in Fig. 2(a), the bottom DBRs are constructed by 12 pairs of dielectric SiO_2/TiO_2 layers with alternative quarter-wavelength thicknesses to guarantee high reflectivity. Notably, in order to reduce the possible strain effect arising from the SiO_2/Si substrate, one layer of SiO_2 was pre-deposited in advance. After the deposition of the bottom DBR, the exfoliated $(PEA)_2PbI_4$ flakes were transferred onto the surface via the Scotch tape method. Subsequently, about 200 nm-thick PMMA was spin-coated on the exfoliated $(PEA)_2PbI_4$ flake for covering the fragile perovskites, preserving their intrinsically optical quality, and merged with the perovskite layer to support Fabry–Pérot oscillation. After that, 11 pairs of SiO_2/Ta_2O_5 layers were deposited on the PMMA as the top DBR. Replacing TiO_2 with Ta_2O_5 here is vital because Ta_2O_5 has a low melting point. Thus, the operating temperature of the *e*-beam evaporation can keep low, which prevents the damage of the delicate gain media. The optical image and the corresponding fluorescence image of the DBR/2D perovskite/DBR sample are shown in Fig. S4, which show the uniform shape and green emission. The cross-sectional scanning electron microscope (SEM) image of the as-fabricated bare cavity is presented in Fig. 2(b), in which the solid dielectric layers can be clearly distinguished, and their interfaces are evident for the alternating structures of the microcavity. As shown in Fig. 2(c), the normalized reflection spectra ranging from 500 to 570 nm of the bottom and top DBRs exhibit their maximum reflectivities of 99.8% and 97.4%, respectively. Such a broad high-reflectivity region of the stop-band covers the complete spontaneous emission of the $(PEA)_2PbI_4$ perovskite and is beneficial to strong optical confinement. In consideration of the incidence of 488 nm excitation laser and the output emission from the top DBR, its reflectivity is designed to be slightly smaller than that of the bottom one. Figure 2(d) shows the emission of the $(PEA)_2PbI_4$ perovskite embedded cavity. Compared with the spontaneous emission band (i.e., located at 527.1 nm with a width of 13.5 nm) of the $(PEA)_2PbI_4$ perovskite on the SiO_2 substrate [Fig. 1(c)], the emission linewidth of the perovskite embedded in the microcavity narrows down to 0.45 nm and redshifts to 537.4 nm, owing to the strong optical confinement of the microcavity. The quality factor Q is estimated by

$$Q = \frac{\lambda}{\Delta\lambda},$$

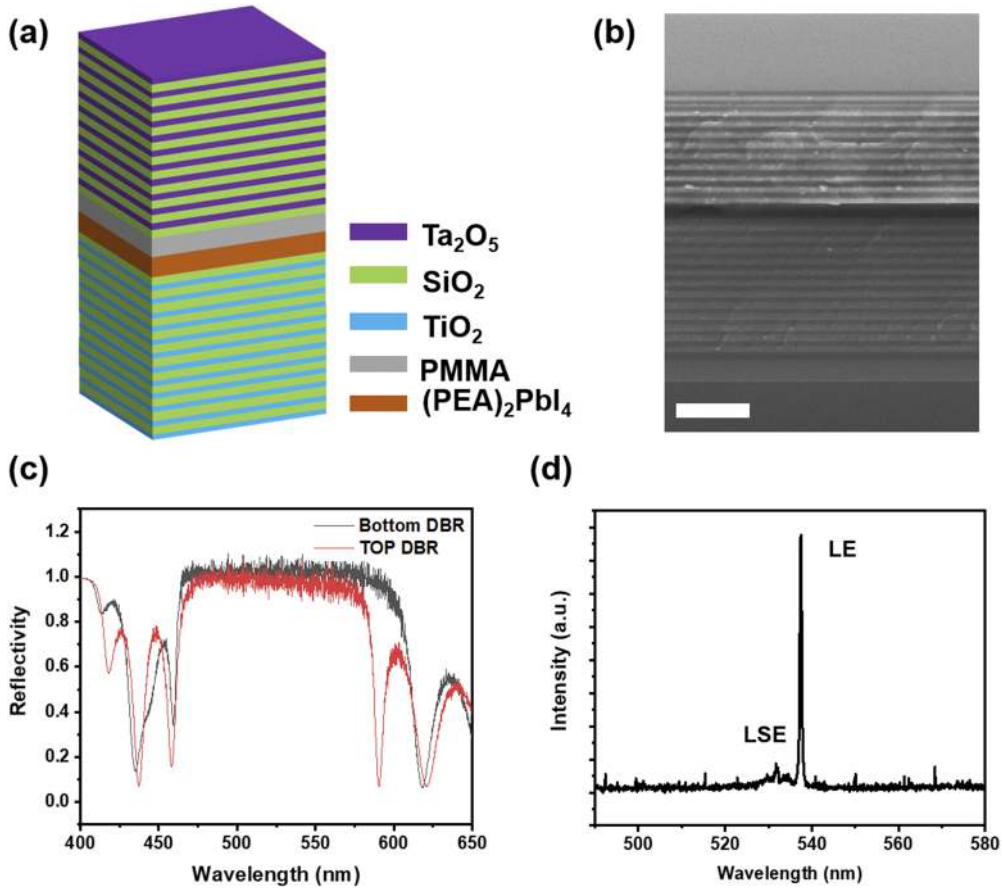

FIG. 2. Construction and characterization of the microcavity. (a) Schematic of the $(PEA)_2PbI_4$ VCSEL, green block: SiO_2 layer, orange block: $(PEA)_2PbI_4$, gray block: PMMA, purple block: Ta_2O_5, and blue block: TiO_2. (b) Classic cross-sectional scanning electron microscope (SEM) image of the microcavity. Scale bar: 1 μm. PMMA locates at the center with a thickness of about 200 nm. (c) Reflectivity spectrum of top DBRs (Ta_2O_5/SiO_2, red trace) and bottom DBRs (TiO_2/SiO_2, black trace). (d) Lasing mode of the $(PEA)_2PbI_4$ embedded microcavity.

where $\Delta\lambda$ and λ represent the width of cavity mode and the emission wavelength, respectively; in our case, the derivative Q is about 1194.

The lasing characteristic of a $(PEA)_2PbI_4$ VCSEL is explored by using a 488 nm CW laser as the pumping source and collecting the emission under the backscattering configuration at room temperature. As presented in Fig. 2(d), a strong lasing emission (LE) peak at 537.4 nm and a weak broad emission band resulting from leaked spontaneous emission (LSE) emerge in the PL spectrum of a $(PEA)_2PbI_4$ VCSEL. Figure 3(a) presents the evolution of the steady-state PL spectra of this perovskite VCSEL sample pumped by various low-excitation powers, ranging from 535 to 540 nm. The emission band raises in intensity and becomes narrower with an increase in excitation power. Figure 3(b) shows the evolution of PL spectra under different high excitation powers in the broad spectral ranges covering all the emission range, where the LSE band is ignorable compared with the LE peak, implying the low optical loss of the VCSEL device. Furthermore, the evolution of the emission peak at 537.4 nm has been explored in detail as the excitation power increases. As shown in Fig. 3(c), the integrated PL emission intensity is plotted as a function of excitation power, which is also called the L–L curve. As the excitation power exceeds a specific value, the PL emission intensity increases remarkably, where such a value is called threshold.[27] Subsequently, lasing emission takes place from the device. From the L–L curve, it is evident that there are two turning points, which divide the curve into three regions categorized as spontaneous emission (SE), superlinear amplification (SLA), and lasing emission, respectively. The SE data (in green) display a sublinear dependence, owing to the reabsorption caused by the reflection of the DBR mirrors and the quenching of exciton emission originating from nonradiative recombination.[14,18,28] The SLA range (in yellow) displays the superlinear feature, while the lasing range (in red) presents the nearly linear behavior. Concisely, this nonlinear characteristic in the L–L curve is the tangible evidence of lasing. A similar transition from sublinear to superlinear has been broadly observed in microcavity lasers based on other large excitonic systems such as 2D transition metal dichalcogenides and organic solid-state crystals.[28,29] Meanwhile, the evolution of the emission peak width

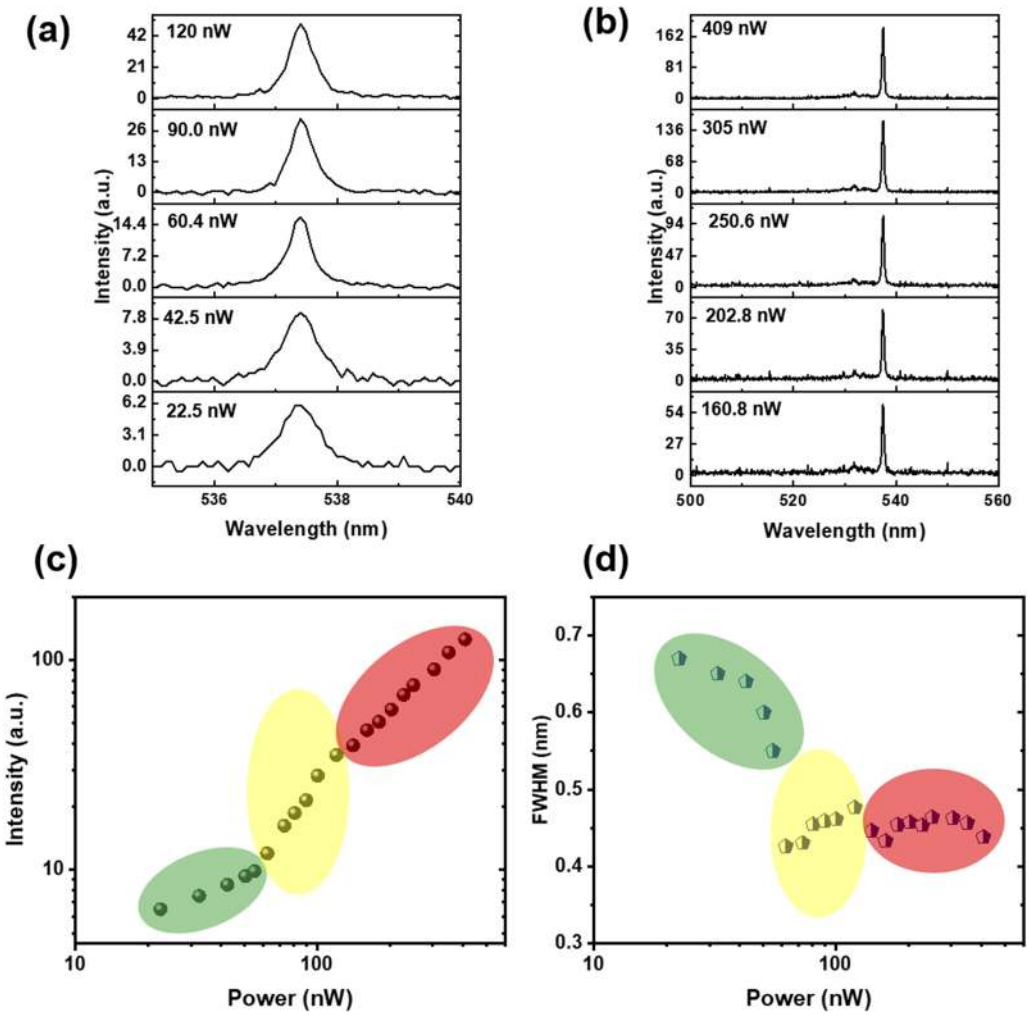

FIG. 3. Lasing characterization of $(PEA)_2PbI_4$ VCSEL. (a) PL spectra collected at the zoom-in range under varied low excitation powers (≤120 nW). (b) PL spectra collected at the extensive range under various high excitation powers (≥160 nW). (c) L–L curve presenting the emission intensity at lasing wavelength as a function of excitation power. (d) Full width at half maximum (FWHM) of the emission as a function of excitation power. The green, yellow, and red regions represent spontaneous emission, superlinear amplification, and lasing.

under the excitation with various powers is present in Fig. 3(d), where it narrows from 0.67 to 0.42 nm during the transition from SE to SLA, with a reducing ratio of 38%. The emission peak is much narrower compared with existing 2D perovskite VCSELs under the pulsed laser pumping, for example, the width of which is 0.8 nm reported by Zhai *et al.*,[10] suggesting a high Q-factor and efficiently optical confinement of our VCSEL device. The similar narrowing of the lasing peak has generally been detected in other 2D perovskite lasers,[10,17,30] which is another suggestive evidence for the evolution from SE to LE. From the change in the intensity and the width with the increasing excitation power, the lasing threshold is extracted at about 65 nW, equivalent to 5.7 W cm^{-2} with an irradiated laser spot size of 1.2 μm, which is one order of magnitude lower than the threshold of the recently reported 2D perovskite CW laser.[18] Such a value is reasonable because perovskites with the preferred crystal orientation usually exhibit a lower threshold.[11,31] For example, a threshold of VCSEL based on the single-crystalline 3D $MAPbBr_3$ perovskite thin film is lately reported as 34 mW cm^{-2}[32] This ultra-low threshold is ascribed to the high quality of the crystalline gain medium and cavity. The spin-coated 2D perovskite thin-film usually contains multiple Ruddlesden–Popper perovskite components, which are easy to form bound excitons and bi-excitons under high-density pumping. In addition, the scattering and the nonradiative recombination at the boundary of the polycrystalline domain could induce optical loss, which hinders the occurrence of lasing. On the contrary, a single crystal with high crystallinity can reduce the defect density efficiently. On the other hand, unlike cavity-free configurations such as nanowire,[9] the designed VCSEL configuration is a useful strategy to promote optical gain. During the fabrication process, the use of PMMA is in favor of the smoother

surface and waveguiding effects. Unlike merely covering the top DBR, which is hard to control the thickness and probably induces additional air gaps, directly depositing the top DBR help for close contact, resulting in a better optical confinement. In contrast, existing CW DFB lasers[18,33] rely on the growth of perovskites as the submicron periodic construction, which produces large scattering loss and leads to larger thresholds.

The stability of emission with continuous excitation is of critical concern for the practical application of a laser device. In order to evaluate the stability of our device, the lasing behavior was monitored via confocal PL measurement along with time. As shown in Fig. 4(a), the as-fabricated $(PEA)_2PbI_4$ VCSEL is under constantly pumping by a 488 nm CW laser with an intensive power of 20 μW for 300 s, and the emission spectra probed from a single pumping spot are illustrated as the contour map of the *in situ* time-dependent PL intensity. A single narrow peak was observed from the spectra without any boarding or shifting over times. Figure 4(b) shows the integrated emission intensity of lasing emission as a function of pump time, where the lasing intensity decreases to 75% of its original value over 300 s. In the previously reported organic–inorganic $MAPbI_3$ perovskite CW laser, the RT lasing emission of which totally vanished after 250 s continuously pumping with the excitation power near the threshold. By contrast, our $(PEA)_2PbI_4$ VCSEL is more stable, owing to the protection afforded by the long-chain PEA cations and surface passivation effects of PMMA.[2,34]

It is worth mentioning, the variation of $(PEA)_2PbI_4$ perovskite layer thickness, unintentionally induced from the exfoliation process, is possible to cause changes in the cavity length, which may lead to multi-mode emission. As shown in Fig. 5(a), the PL spectra of $(PEA)_2PbI_4$ VCSEL in a broad range exhibit two narrow emission peaks located at 538.3 and 539.8 nm, denoted as mode 1 and mode 2, respectively. Both modes rise with the increase in pumping power. LSE is relatively low, indicating the lasing fraction is dominating. The mode spacing between modes 1 and 2 is 1.5 nm. If we assume this 1.5 nm spacing is free spectral range of a Fabry–Pérot resonator, which is defined as

$$\Delta\lambda_{FSR} = \frac{\lambda^2}{2nL},$$

where λ represents the wavelength of the resonated optical wave in vacuum, n denotes the group refractive index, and L stands for the length of the cavity. In our designed cavity, $\Delta\lambda_{FSR}$ can be deviated as

$$\Delta\lambda_{FSR} = \frac{\lambda^2}{2n_{\mathrm{Pero}}L_{\mathrm{Pero}} + 2n_{\mathrm{PMMA}}L_{\mathrm{PMMA}}},$$

where n_{Pero} and n_{PMMA} denote the refractive index of $(PEA)_2PbI_4$ perovskite and PMMA and L_{Pero} and L_{PMMA} stand for the thickness of $(PEA)_2PbI_4$ perovskite and PMMA, respectively.

If we take

$$\Delta\lambda_{FSR} = 1.5 \text{ nm},$$

then the thickness of the $(PEA)_2PbI_4$ perovskite can be calculated as

$$L_{Pero} = 44\ \mu\text{m},$$

which is two orders of magnitude larger than our designed thickness, even much larger than the lateral size. Therefore, we assigned these two modes to the emission that originated from perovskite flakes with slightly various thicknesses. The power-dependent PL measurement has been conducted for detailed studies. As shown in Fig. 5(b), the L–L curve of mode 1 exhibits the kink point pronouncedly, which appears around 307 nW. The regions of SE, SLA, and LE can be identified clearly. Figure 5(c) presents a similar evolution of mode 2, but the extracted threshold is at 110 nW. The different thresholds of these two modes indicate that they are originated from perovskite flakes with different thicknesses, i.e., the cavity length is changed. Thus, the thresholds are different due to the change in the dielectric environment.

The wavelength of the cavity mode is greatly dependent on the cavity length. In order to explore the relation between the thickness of the $(PEA)_2PbI_4$ flake and the position of the cavity mode, the simulated reflection spectrum of our designed cavity structure with the perpendicular incidence was theoretically calculated with the finite-difference time-domain (FDTD) method. The simulated VCSEL structures were set to consist of 200 nm PMMA and one $(PEA)_2PbI_4$ layer with thicknesses of 243, 245,

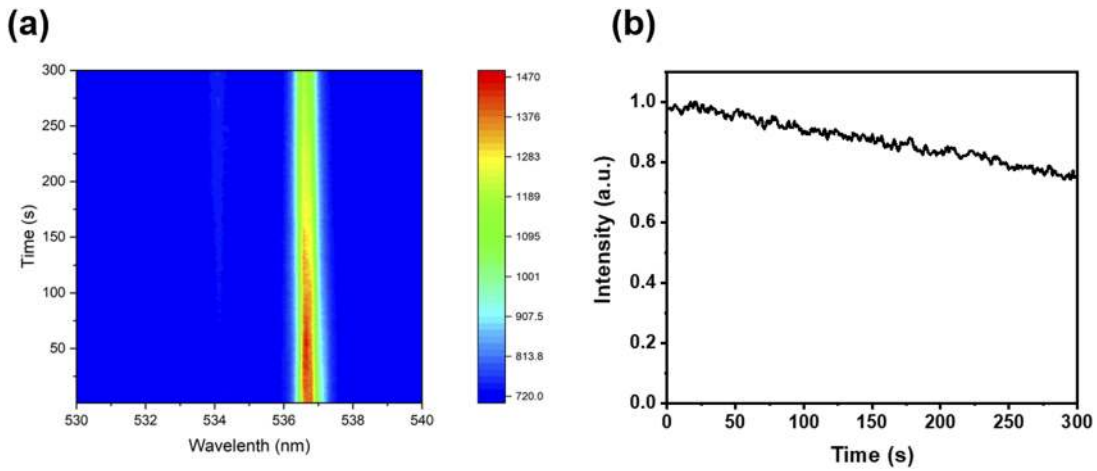

FIG. 4. Stability of as-fabricated $(PEA)_2PbI_4$ VCSEL under constant excitation. (a) Contour map of the time-dependent PL intensity. (b) Integrated emission intensity of lasing emission as a function of pumping time at room-temperature ambient atmosphere. The excitation is the 488 nm CW laser with a power of 12 μW.

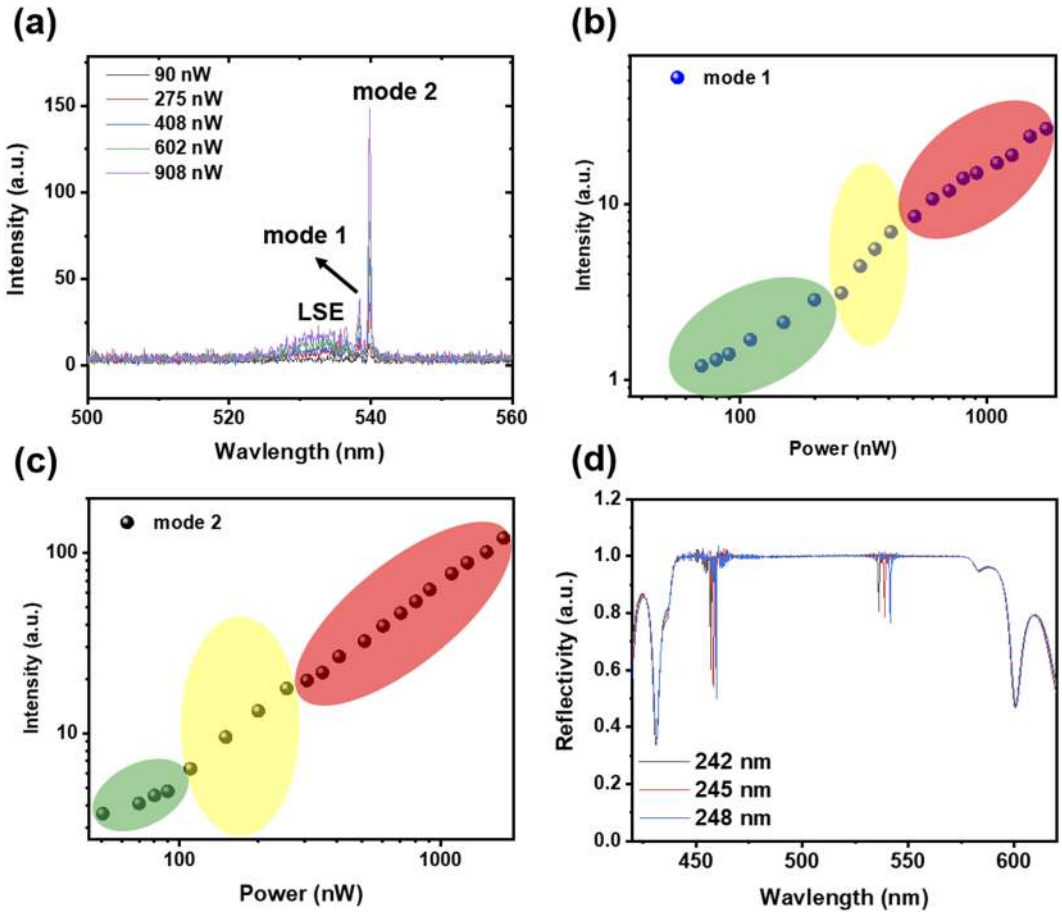

FIG. 5. Lasing characterization of as-fabricated $(PEA)_2PbI_4$ VCSEL with two lasing modes. (a) PL spectra collected under a variety of excitation powers. [(b) and (c)] Intensity of PL emission of two modes as a function of excitation power. The green, yellow, and red regions represent spontaneous emission, superlinear amplification, and lasing, respectively. (d) Simulated reflection spectrum of as-designed VCSEL with various thickness of $(PEA)_2PbI_4$ flakes.

and 248 nm, respectively. Thus, it is understandable that there are two modes in the spectrum [Fig. 5(d)]. However, only the mode at the long wavelength side will be observed from PL spectra because the mode located at about 460 nm is out of the emission range of $(PEA)_2PbI_4$. The wavelength of the cavity photon was designed to locate at the lower energy side of the emission range, considering the higher absorption at the higher energy side. As the thickness of the $(PEA)_2PbI_4$ layer slightly increases, the cavity mode redshifts synchronously. The modes at the long-wavelength side of the cavities with 243, 245, and 248 nm $(PEA)_2PbI_4$ layers are 536.1, 538.8, and 541.5, respectively. Obviously, the step of the redshift with an increase of 3 nm in thickness is 2.7 nm. Therefore, we consider the mode spacing between modes 1 and 2 in Fig. 5(a) as 1.5 nm, which can be attributed to the roughness of the exfoliated $(PEA)_2PbI_4$ flakes' surface, leading to the difference in thickness as well as the change in cavity length.

In summary, millimeter-sized high-quality 2D layered $(PEA)_2PbI_4$ single crystals have been successfully synthesized by a modified two-step seed-growth method, the mechanically exfoliated thin flakes of which exhibit high crystallization, excellent thermally stability, and outstanding optical properties. The exfoliated $(PEA)_2PbI_4$ flakes were utilized as the superior gain materials and embedded in two sets of high-reflectivity DBRs to form a high Q-factor VCSEL. The single-mode CW lasing with an ultra-low threshold of 5.7 W cm^{-2} has been observed at room temperature, which is demonstrated by the intensity kink of the L–L curve and the linewidth narrowing. The as-fabricated laser displays improved photostability with a working duration of over 300 s, which is much more stable compared with the relevant 3D perovskite laser.[33] The multi-mode emission has been synchronously explored, attributed to the roughness induced unintentionally during the exfoliation process. This work is not only beneficial to the development of electrically driven laser based on 2D lead halide perovskites but also truly pushes the field of practical coherent light sources and on-chip integrated optics.

SUPPLEMENTARY MATERIAL

See the supplementary material for experimental details.

AUTHORS' CONTRIBUTIONS

H.Z. and Y.H. contributed equally to this work.

ACKNOWLEDGMENTS

This research was supported by the Ministry of Education of Singapore Tier 2 (Grant Nos. MOE2018-T2-2-072 and MOE 2019-T2-1-044) and Academic Research Fund Tier 1 (Grant No. RG93/19) and the National Research Foundation-Competitive Research Program (Grant Nos. NRF-CRP21-2018-0007). H.J.F. would like to acknowledge support from the Agency for Science, Technology, and Research (A*STAR) by AME Individual Research Grant (No. A1883c0004). J.S. acknowledges support from the Fundamental Research Funds for the Central Universities of China, the National Natural Science Foundation of China (Grant No. 61904151), the Natural Science Foundation of Shaanxi (Grant No. 2020JM-108), and the Joint Research Funds of Department of Science and Technology of Shaanxi Province and Northwestern Polytechnical University (Grant No. 2020GXLH-Z-020). S.F. was supported by the H2020-MSCA-IF-2020 project SingExTr (Grant No. 101031596).

DATA AVAILABILITY

The data that support the findings of this study are available from the corresponding author upon reasonable request.

REFERENCES

[1]J. H. Noh, S. H. Im, J. H. Heo, T. N. Mandal, and S. I. Seok, Nano Lett. **13**(4), 1764 (2013); M. L. Agiorgousis, Y.-Y. Sun, H. Zeng, and S. Zhang, J. Am. Chem. Soc. **136**(41), 14570 (2014).

[2]K. Leng, I. Abdelwahab, I. Verzhbitskiy, M. Telychko, L. Chu, W. Fu, X. Chi, N. Guo, Z. Chen, Z. Chen, C. Zhang, Q.-H. Xu, J. Lu, M. Chhowalla, G. Eda, and K. P. Loh, Nat. Mater. **17**(10), 908 (2018).

[3]K. Wang, C. Wu, D. Yang, Y. Jiang, and S. Priya, ACS Nano **12**(5), 4919 (2018). Z. Tan, Y. Wu, H. Hong, J. Yin, J. Zhang, L. Lin, M. Wang, X. Sun, L. Sun, Y. Huang, K. Liu, Z. Liu, and H. Peng, J. Am. Chem. Soc. **138**(51), 16612 (2016).

[4]M. Yuan, L. N. Quan, R. Comin, G. Walters, R. Sabatini, O. Voznyy, S. Hoogland, Y. Zhao, E. M. Beauregard, P. Kanjanaboos, Z. Lu, D. H. Kim, and E. H. Sargent, Nat. Nanotechnol. **11**(10), 872 (2016); N. Wang, L. Cheng, R. Ge, S. Zhang, Y. Miao, W. Zou, C. Yi, Y. Sun, Y. Cao, R. Yang, Y. Wei, Q. Guo, Y. Ke, M. Yu, Y. Jin, Y. Liu, Q. Ding, D. Di, L. Yang, G. Xing, H. Tian, C. Jin, F. Gao, R. H. Friend, J. Wang, and W. Huang, Nat. Photonics **10**(11), 699 (2016).

[5]J.-C. Blancon, J. Even, C. C. Stoumpos, M. G. Kanatzidis, and A. D. Mohite, Nat. Nanotechnol. **15**(12), 969 (2020).

[6]X. Gao, X. Zhang, W. Yin, H. Wang, Y. Hu, Q. Zhang, Z. Shi, V. L. Colvin, W. W. Yu, and Y. Zhang, Adv. Sci. **6**(22), 1900941 (2019).

[7]K. Leng, W. Fu, Y. Liu, M. Chhowalla, and K. P. Loh, Nat. Rev. Mater. **5**(7), 482 (2020).

[8]M. R. Leyden, T. Matsushima, C. Qin, S. Ruan, H. Ye, and C. Adachi, Phys. Chem. Chem. Phys. **20**(22), 15030 (2018); M. Li, Q. Wei, S. K. Muduli, N. Yantara, Q. Xu, N. Mathews, S. G. Mhaisalkar, G. Xing, and T. C. Sum, Adv. Mater. **30**(23), e1707235 (2018); E. P. Booker, M. B. Price, P. J. Budden, H. Abolins, Y. del Valle-Inclan Redondo, L. Eyre, I. Nasrallah, R. T. Phillips, R. H. Friend, F. Deschler, and N. C. Greenham, Adv. Opt. Mater. **6**(21), 1800616 (2018); J. M. Pina, D. H. Parmar, G. Bappi, C. Zhou, H. Choubisa, M. Vafaie, A. M. Najarian, K. Bertens, L. K. Sagar, Y. Dong, Y. Gao, S. Hoogland, M. I. Saidaminov, and E. H. Sargent, Adv. Mater. **33**, 2006697 (2020).

[9]H. Zhang, Y. Wu, Q. Liao, Z. Zhang, Y. Liu, Q. Gao, P. Liu, M. Li, J. Yao, and H. Fu, Angew. Chem., Int. Ed. Engl. **57**(26), 7748 (2018).

[10]W. Zhai, C. Tian, K. Yuan, C. Ge, S. Zhao, H. Yu, Y. Li, W. Chen, and G. Ran, Appl. Phys. Lett. **114**(13), 131107 (2019).

[11]L. Lei, D. Seyitliyev, S. Stuard, J. Mendes, Q. Dong, X. Fu, Y. A. Chen, S. He, X. Yi, L. Zhu, C. H. Chang, H. Ade, K. Gundogdu, and F. So, Adv. Mater. **32**(16), 1906571 (2020).

[12]M. Li, Q. Gao, P. Liu, Q. Liao, H. Zhang, J. Yao, W. Hu, Y. Wu, and H. Fu, Adv. Funct. Mater. **28**(17), 1707006 (2018).

[13]M. R. Leyden, S. Terakawa, T. Matsushima, S. Ruan, K. Goushi, M. Auffray, A. S. D. Sandanayaka, C. Qin, F. Bencheikh, and C. Adachi, ACS Photonics **6**(2), 460 (2019).

[14]H. Zhang, Q. Liao, Y. Wu, Z. Zhang, Q. Gao, P. Liu, M. Li, J. Yao, and H. Fu, Adv. Mater. **30**(15), 1706186 (2018).

[15]W. B. Gunnarsson and B. P. Rand, Appl. Mater. **8**(3), 030902 (2020); B. R. Sutherland and E. H. Sargent, Nat. Photonics **10**(5), 295 (2016).

[16]C. M. Raghavan, T.-P. Chen, S.-S. Li, W.-L. Chen, C.-Y. Lo, Y.-M. Liao, G. Haider, C.-C. Lin, C.-C. Chen, R. Sankar, Y.-M. Chang, F.-C. Chou, and C.-W. Chen, Nano Lett. **18**(5), 3221 (2018).

[17]L. Yin, Q. Shang, W. Qi, L. Zhao, Z. Liu, S. Jia, Y. Zhong, J. Chen, Y. Gao, M. Li, X. Liu, G. Xing, and Q. Zhang, Adv. Mater. **31**(39), 1903030 (2019).

[18]C. Qin, A. S. D. Sandanayaka, C. Zhao, T. Matsushima, D. Zhang, T. Fujihara, and C. Adachi, Nature **585**(7823), 53 (2020).

[19]B. Wu, H. T. Nguyen, Z. Ku, G. Han, D. Giovanni, N. Mathews, H. J. Fan, and T. C. Sum, Adv. Energy Mater. **6**(14), 1600551 (2016); Z. Ku, N. H. Tiep, B. Wu, T. C. Sum, D. Fichou, and H. J. Fan, New J. Chem. **40**(9), 7261 (2016).

[20]H. Li, J. Song, W. Pan, D. Xu, W. Zhu, H. Wei, and B. Yang, Adv. Mater. **32**(40), 2003790 (2020).

[21]Y. Liu, H. Ye, Y. Zhang, K. Zhao, Z. Yang, Y. Yuan, H. Wu, G. Zhao, Z. Yang, J. Tang, Z. Xu, and S. Liu, Matter **1**(2), 465 (2019).

[22]F. Lédée, G. Trippé-Allard, H. Diab, P. Audebert, D. Garrot, J.-S. Lauret, and E. Deleporte, CrystEngComm **19**(19), 2598 (2017); Y. Tu, Y. Xu, J. Li, Q. Hao, X. Liu, D. Qi, C. Bao, T. He, F. Gao, and W. Zhang, Small **16**, 2005626 (2020).

[23]D. H. Cao, C. C. Stoumpos, O. K. Farha, J. T. Hupp, and M. G. Kanatzidis, J. Am. Chem. Soc. **137**(24), 7843 (2015).

[24]B. Dan, Y. Wang, J. Bai, R. Du, G. Wu, and L. Liu, Opt. Commun. **406**, 128 (2018).

[25]V. A. Dragomir, S. Neutzner, C. Quarti, D. Cortecchia, A. Petrozza, S. Roorda, D. Beljonne, R. Leonelli, A. R. Srimath Kandada, and C. Silva, arXiv:1812.05255 (2018); J. Yin, P. Maity, R. Naphade, B. Cheng, J.-H. He, O. M. Bakr, J.-L. Brédas, and O. F. Mohammed, ACS Nano **13**(11), 012621 (2019).

[26]F. Thouin, D. A. Valverde-Chávez, C. Quarti, D. Cortecchia, I. Bargigia, D. Beljonne, A. Petrozza, C. Silva, and A. R. Srimath Kandada, Nat. Mater. **18**(4), 349 (2019).

[27]W. Demtröder, *Laser Spectroscopy*, 4th ed. (Springer, Berlin, 2008).

[28]J. Shang, C. Cong, Z. Wang, N. Peimyoo, L. Wu, C. Zou, Y. Chen, X. Y. Chin, J. Wang, C. Soci, W. Huang, and T. Yu, Nat. Commun. **8**(1), 543 (2017).

[29]K. Yamashita, T. Nakahata, T. Hayakawa, Y. Sakurai, T. Yamao, H. Yanagi, and S. Hotta, Appl. Phys. Lett. **104**(25), 253301 (2014).

[30]P. Bouteyre, H. Son Nguyen, J.-S. Lauret, G. Trippé-Allard, G. Delport, F. Lédée, H. Diab, A. Belarouci, C. Seassal, D. Garrot, F. Bretenaker, and E. Deleporte, Opt. Express **28**(26), 39739 (2020).

[31]R. Wang, Y. Tong, A. Manzi, K. Wang, Z. Fu, E. Kentzinger, J. Feldmann, A. S. Urban, P. Müller-Buschbaum, and H. Frielinghaus, Adv. Opt. Mater. **6**(6), 1701311 (2018).

[32]C. Tian, T. Guo, S. Zhao, W. Zhai, C. Ge, and G. Ran, RSC Adv. **9**(62), 35984 (2019).

[33]Z. Li, J. Moon, A. Gharajeh, R. Haroldson, R. Hawkins, W. Hu, A. Zakhidov, and Q. Gu, ACS Nano **12**(11), 10968 (2018).

[34]M. S. Alias, Z. Liu, A. Al-Atawi, T. K. Ng, T. Wu, and B. S. Ooi, Opt. Lett. **42**(18), 3618 (2017).